

# Effects of Laser Repetition Rate on Corneal Tissue Ablation for 193-nm Excimer Laser Light

Leia M. Shanyfelt, MS,<sup>1</sup> Pamela L. Dickrell, PhD,<sup>1</sup> Henry F. Edelhauser, PhD,<sup>2</sup> and David W. Hahn, PhD<sup>1\*</sup>

<sup>1</sup>College of Engineering, University of Florida, Gainesville, Florida 32611

<sup>2</sup>Department of Ophthalmology, Emory University School of Medicine, Atlanta, Georgia 30322

**Background and Objective:** The goal of the present work is to assess whether bovine corneal ablations generated at laser repetition rates of up to 400 Hz are comparable to ablations performed at rates consistent with current clinical laser systems.

**Study Design/Materials and Methods:** A combination of experiments was used to assess a comprehensive range of ablation parameters, including ablation plume dynamics via imaging and transmission, corneal ablation profiles via scanning interferometry, and high-resolution electron microscopy of collagen structure following ablation.

**Results:** Using white-light interferometry analysis, no statistical difference was found between corneal ablation profiles created at 60 and 400 Hz, with an average rate of 0.94  $\mu\text{m}/\text{pulse}$  at 60 Hz versus 0.92  $\mu\text{m}/\text{pulse}$  at 400 Hz. In addition, based on plume imaging and transmission studies, the bulk ablation plume was found to dissipate on a time-scale less than the pulse-to-pulse separation for a laser repetition rate up to about 400 Hz. A persistent, diffuse gas-phase component of the ablation products was observed and concluded to be comparable at both repetition rates. Finally, SEM and TEM analysis revealed no signs of differential thermal tissue damage, including collagen fibril analysis, for laser repetition rates up to 400 Hz.

**Conclusions:** In summary, investigation of the relative effects of excimer laser repetition rate on the overall corneal ablation metrics revealed no measurable difference under conditions typical of clinical refractive procedures. This study suggests that increases in ArF laser repetition rates for clinical applications (up to  $\sim 400$  Hz) appear feasible. *Lasers Surg. Med.* 40:483–493, 2008.

© 2008 Wiley-Liss, Inc.

**Key words:** refractive; LASIK; PRK; interferometry; plume; collagen; TEM

## INTRODUCTION

Excimer laser refractive surgery is a very popular option for vision correction. As demand for the procedure has increased, the surgical procedures and devices have evolved, although laser photorefractive surgery continues to be studied for ways to improve clinical outcome and convenience. Accordingly, both accuracy and precision, as well as patient comfort, must be considered. Toward these ends, increases in laser repetition rate, and the corresponding reduction in procedure time, are of practical interest,

notably with greater diopter corrections. The goal of the present work is to assess whether corneal ablations generated at a laser repetition rate of up to 400 Hz are equivalent to ablations performed at current surgical laser repetition rates. A review of current FDA-approved LASIK laser systems indicates that surgeries using a 193-nm ArF excimer laser are performed between 1.5 and 250 Hz, depending on the manufacturer and model of the system [1]. This is an extensive range of operation, especially when one considers that there are several other conditions that vary as well, including laser spot size, average and peak laser fluence, and the overall beam steering algorithms (e.g., wide field vs. flying spot approach) [2].

A thorough understanding of the physics and mechanisms of corneal ablation and the potential role of laser repetition rate remains a topic of research [3–9]. As the exact mechanisms of photoablation remain unidentified, it is critical to show that increasing the laser repetition rate does not reveal any differences in surgical outcome or underlying corneal pathology. The laser–tissue interaction may be generalized as a dynamic process during which the corneal optical properties are perturbed by the laser beam during the time-course of the ablating laser pulse. Photocleavage of collagen fibrils and proteoglycans leads to subsurface expansion of the corneal tissue matrix and subsequent stress that drives the ablated tissue from the surface in the form of the well-known ablation plume [10–14]. Critical questions regarding potential laser rate effects include the possibility of changes in laser–plume interactions, differences in the kinetics of laser–tissue coupling resulting in different ablation rates, and potential damage to the tissue underlying the ablation zone.

With each laser pulse, the ablated corneal material is ejected from the eye surface as the ablation plume. It is essential to examine the dynamics of this plume to determine if the physical removal of tissue during ablation is altered as the laser pulse rate is increased to values higher than current clinical rates. Excess material

Contract grant sponsor: Alcon Research, Ltd. and in part (HFE) by NEI grants R01-EY00933 and P30-EY06360.

\*Correspondence to: David W. Hahn, PhD, Mechanical and Aerospace Engineering, University of Florida, PO Box 116300, Gainesville, FL 32611. E-mail: dwhahn@ufl.edu

Accepted 20 May 2008

Published online in Wiley InterScience  
(www.interscience.wiley.com).

DOI 10.1002/lsm.20656

lingering over the surgical plane could alter the ablation process, notably by attenuating the laser pulse energy and thereby decreasing the amount of corneal tissue removed. Also, the excess material may settle back down onto the corneal surface, also resulting in under-ablation of the cornea [15,16]. Accordingly, it is desirable that the ablation rate provide adequate time for the ablation plume from one shot to sufficiently dissipate before the next laser shot occurs.

To ensure successful clinical outcome, it is crucial that the overall ablation profiles generated at the relevant laser repetition rates are statistically identical for a given refractive correction. The ablation depth generated by a particular system is a function of the incident laser fluence, with higher fluences producing deeper ablation depths. A wide range of reported experimental data has been summarized and plotted by Fisher et al., and indicates laser fluences ranging from about 25 to 700 mJ/cm<sup>2</sup> with corresponding ablation rates from threshold to about 1.4 μm/pulse [10,17–25]. A review of current FDA-approved LASIK systems reveals a wide variety of average laser fluences on the market, ranging from about 100 to 250 mJ/cm<sup>2</sup>, although the peak fluence with Gaussian beams may be in excess of 500 mJ/cm<sup>2</sup> [1].

The corneal stroma is made up of approximately 75% water and about 20% collagen and proteoglycans (dermatan and keratan sulfates). The collagen structure consists of regularly spaced collagen fibrils which are of approximately equal diameter, arranged in layers of parallel lamellae. The stroma ranges in thickness from about 0.5 to 0.7 mm, based on the distance from the center of the eye. The corneal stroma is made up of about 300–500 lamellae (bundles) of parallel fibrils, with each bundle of fibrils arranged parallel to the adjacent bundle [26–28]. The reported values of the diameter of the fibrils ranges considerably, namely from 20 to 34 nm, and in the central region of the cornea, the diameter is considered independent of corneal hydration [26–29].

When ablated, the immediate corneal stroma becomes disrupted and may become thermally damaged. Notably, at temperatures above approximately 60°C, coagulation and denaturing of collagen can occur. These effects can be observed using microscopy, showing disruptions in the collagen structure and an aggregation of fibrils. This would cause the interfibrillar distance at the ablation surface to shorten, and thus the density and cross-sectional area of collagen fibrils would be expected to increase [30,31]. The level of disorganization and fiber densification observed with high-resolution microscopy may therefore be considered a measure of thermal damage to the underlying tissue [31]. Venugopalan et al. [32] attempted to model the effect of various laser parameters, including pulse duration and laser irradiance, to determine the zone of thermal energy as a function of the Péclet number. Unfortunately, a lack of knowledge of the ablation mechanism limited the model, as acknowledged by the authors. A model of thermal damage induced by 193-nm irradiation that takes into account current understandings, including dynamic optical properties and Beer–Lambert law deviation, still remains

unavailable. Nonetheless, thermal damage should be considered in the context of higher laser repetition rates, as less time is available between laser shots for energy to dissipate via conduction within the corneal stroma.

These issues form the basis of the present investigation into laser repetition rates effects on laser refractive surgery. In addition, differences in healing response following refractive surgery may result from changes in ablation rates. Such effects are beyond the scope of the present study, but rather are suggested as follow-up studies.

## MATERIALS AND METHODS

In all experiments, whole bovine eye globes were extracted immediately following sacrifice (less than 20 minutes) and placed in sealed, buffered saline solution-filled plastic bags and kept at room temperature. Experiments were always performed within several hours following animal sacrifice. Prior to all ablations, the corneal surface was mechanically de-epithelialized using a scalpel edge.

For all experiments, the 193-nm ArF excimer laser (Coherent TuiLaser, Santa Clara, CA) was used for the corneal ablations. The laser output energy was set to 2.7 mJ per pulse at the corneal eye plane and the spot size was approximately 1 mm. A comparable laser platform is currently used in FDA-approved clinical systems at rates between 60 and 100 Hz utilizing an identical treatment algorithm. The laser is capable of producing laser repetition rates from 1 Hz to above 400 Hz. Alcon proprietary software controlled the delivery of a specified refractive correction over a 6-mm treatment zone. Essentially, the laser beam is rastered over the cornea surface using a series of overlapping, spiraling arcs. As in clinical settings, the laser beam was oriented downward onto the bovine eye. The surgical 193-nm ArF excimer laser beam (denoted Laser 1) passes through a beam homogenizer, a focusing lens and a pinhole before entering the scan cube, as shown in Figure 1. The scan cube contains two orthogonal mirrors that move in concert to generate a correction profile at the corneal plane. After exiting the scan cube, the beam then passes through a second focusing lens and two mirrors and is projected downward onto the corneal surface. The bovine eye globe was held in a specially designed holder to keep it static and taut during the procedure. The intraocular pressure was not measured in this set of experiments but is considered comparable to normal physiological pressures. The eye holder was specifically designed to keep a consistent, minimal pressure on all eyes. The purpose of keeping the eye surface taut was to prevent aberrations in the ablation profile due to distortion of the bovine eyes, which naturally occurs following excision. It is noted that enucleated eyes tend to wrinkle and/or sag on the corneal surface; hence the eye holder restores the corneal surface of the whole globes to a more natural state.

## Ablation Plume Imaging

To assess the ablation plume dynamics, planar laser light scattering measurements were performed. An Andor iStar

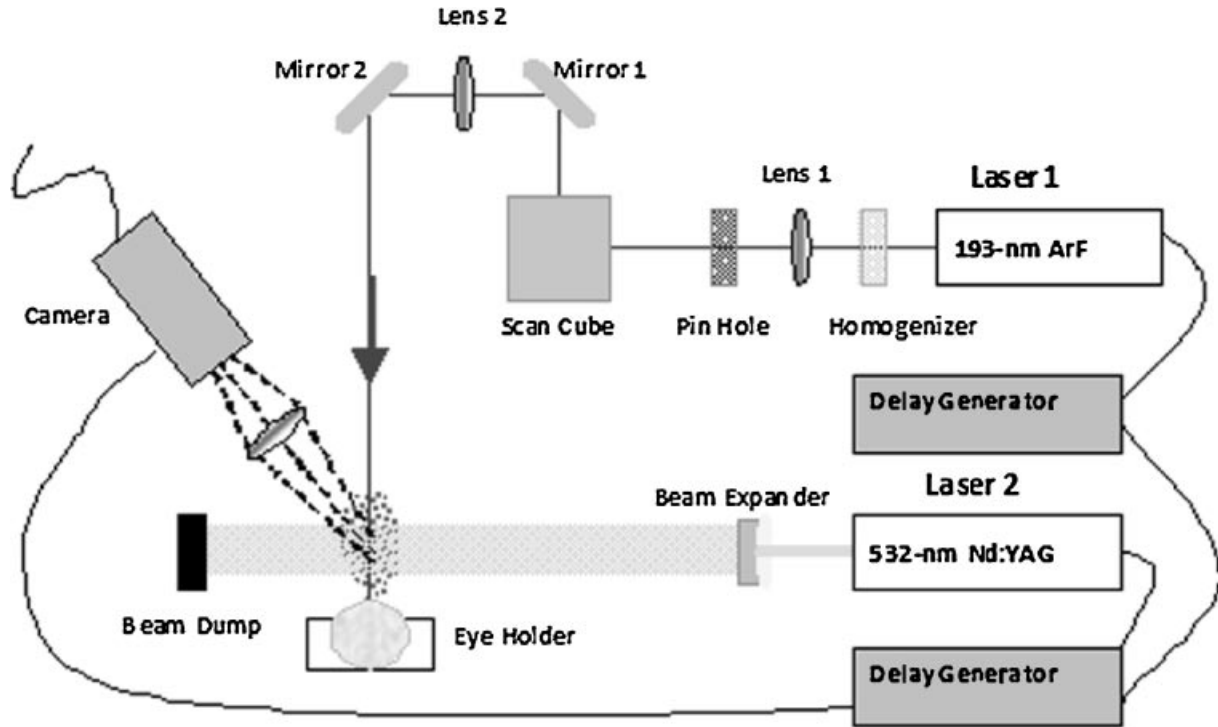


Fig. 1. Schematic of the experimental configuration for measuring ablation plume dynamics.

CCD camera (1,024×1,024 pixels) was used to record images of the plume. For imaging, an Nd:YAG pulsed solid-state laser (Laser 2) at 532 nm was used to illuminate the plume, as shown in Figure 1. A cylindrical lens was used to create a vertical sheet of light which passed above the corneal surface normal to the camera. Using digital delay generators, the pulsed Nd:YAG light was synchronized to the ablating excimer laser pulse. By adjusting the delay between the two lasers, the temporal evolution of the ablation plume was imaged for delays ranging from 120 microseconds to 40 milliseconds following the excimer laser pulse, noting that a delay time of zero corresponds to coincident laser pulses. The method of using scattered light to image an ablation plume is well documented and dates back to the pioneering work of Puliafito and coworkers [16,33,34].

### Transmission

To further analyze the ablation plume evolution, a second 193-nm ArF laser beam was used to probe the ablation plume, including interactions with solid phase (i.e., particulate) and gas phase components.

The path of the surgical ArF laser (Laser 1) for these studies was identical to that described above for the imaging studies. The transmission probe ArF excimer laser beam (GAM Laser, Inc., Orlando, FL), labeled as Laser 3, was split into two paths, considered the incident and transmitted, using a glass quartz flat as a beam splitter, as shown in Figure 2. The incident beam path passes through the quartz flat, then through a set of neutral density filters

to ensure signal linearity, a pin hole to minimize stray light, a 193-nm line filter to eliminate any laser-induced fluorescence signal, and finally into the detector (200-picoseconds rise-time photodiode). The transmitted beam path follows a similar path of optics but is passed through the center of the ablation plume at a height of 2 mm above the corneal surface. Figure 2 demonstrates the configuration used for this set of experiments. This general method has been successfully implemented in the analysis of ablation plume dynamics [34].

The incident probe signal was compared to the transmitted signal to determine the transmission. The ratio of the integrated transmitted signal to the integrated incident signal normalized to the ratio with no plume present defines the transmission. The transmission of light through the ejected plume may be coupled with the plume images to assess whether the material removal mechanism is affected by residual plume material from previous laser shots. In general terms, the transmission is defined as

$$\tau = \frac{I(\ell)}{I_0} \quad (1)$$

where  $I(\ell)$  is the intensity of the laser light after passing through the plume path length,  $\ell$ , and  $I_0$  is the incident laser intensity. Thus, the normalized ratio (i.e., plume/no plume) is the transmission through the ablation plume. Using digital delay generators, the transmission of the plume was determined as a function of time with respect to Laser 1, as in the plume dynamics study above, for delays ranging from 0 microseconds to 1 milliseconds.

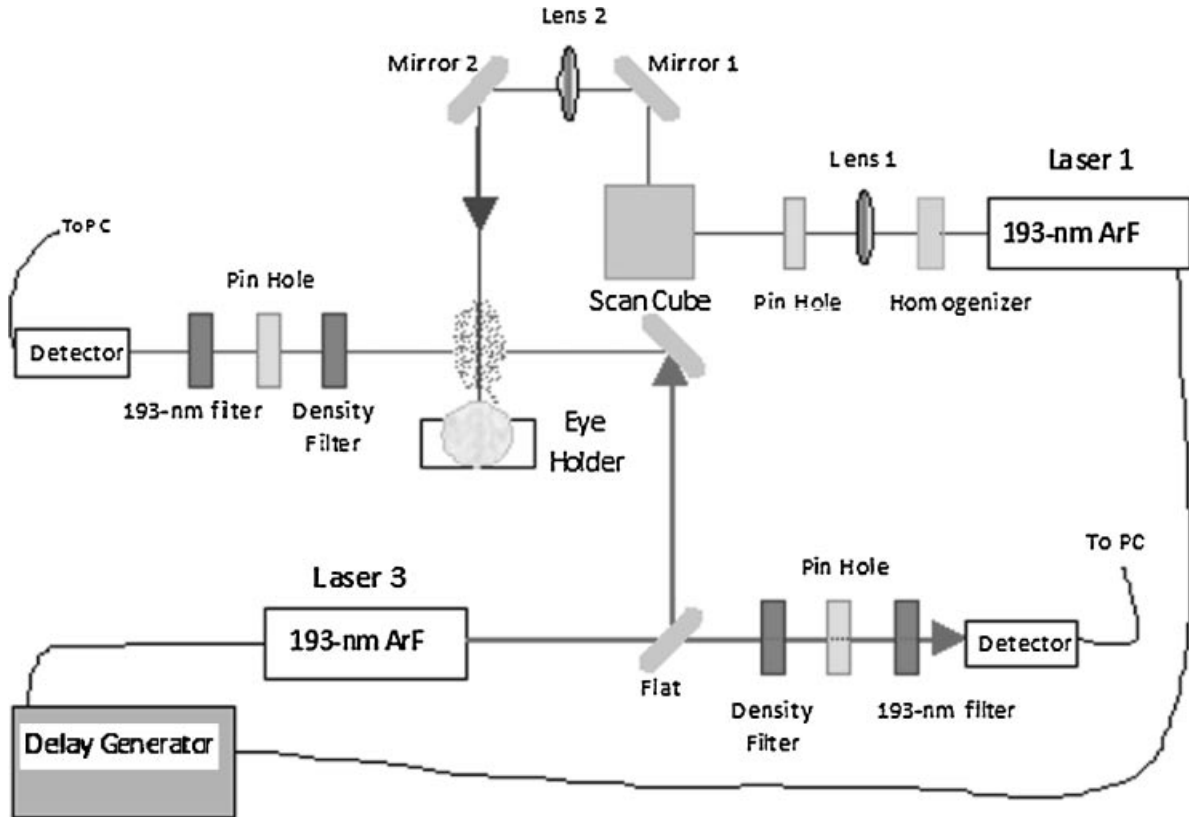


Fig. 2. Schematic of the experimental configuration for the plume transmission study.

### Ablation Profile

In order to assess any variations in the ablation profiles generated by varying the laser repetition rate, corneal tissue ablation craters were analyzed. Ablation craters were generated by interdispersing a 25-shot sequence (evenly dispersed throughout the treatment algorithm) onto the center of a 3-diopter, 6-mm zone ablation treatment, as shown in Figure 3. The 3-diopter, 6-mm zone ablation treatment is representative of a typical moderate correction for this surgical laser system. These ablations were performed with the laser operating at either 60 Hz (based on existing clinical rates) or 400 Hz using paired eyes from each bovine. Hence, one eye received the treatment at 60 Hz, and the second eye received the treatment at 400 Hz. Using interdispersed shots on a standard profile provided a more clinical representation than a simple static laser

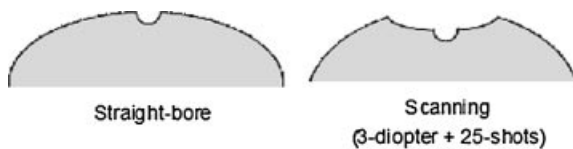


Fig. 3. Schematic cross-sections of the ablation patterns generated by the straight-bore and scanning algorithms. The scanning algorithm shows the additional 25-shot pulse sequence superimposed on a 3-diopter profile.

beam because in clinical applications the time between laser pulses at a given location is significantly greater than the pulse-to-pulse firing time due to the scanning algorithm employed by the laser system. Immediately following completion of the ablation, impressions of the craters were prepared using single drops of paraffin wax as previously documented [35]. Once the wax was thoroughly solidified, the impression was inverted and transferred to a microscope slide. A Zygo NewView white-light interferometer was used to obtain three-dimensional surface profiles of the full craters. The interferometer was outfitted with a  $5\times$  Michelson objective with a  $0.5\times$  magnification setting resulting in a net  $2.5\times$  surface view. Five eyes were analyzed at each laser repetition rate (10 eyes total).

In order to process the images, six two-dimensional cross-sections were extracted from each three-dimensional interferogram using a star pattern such that each cross-section bisected the center of the ablation crater. Parabolic trend lines, which provided good approximations of the corneal surface near the ablation site, were used to subtract the overall corneal surface curvature from each cross-section, yielding the ablation profiles. The six cross-sections were then averaged to yield the final 2D ablation profile for each treated cornea.

### Histology

To assess any histological changes to the underlying stroma caused by varying the laser repetition rate, corneal

ablations were performed over a 6-mm zone with a standard 9-diopter correction, the maximum correction typically applied for this surgical system, using laser repetition rates of 60 and 400 Hz. This 9-diopter correction is considered a worst case from a histological perspective, as it produces the maximum number of laser pulses, and therefore, the maximum possible potential for tissue damage. For these experiments, no additional laser shots were added in the center as was done in the ablation profile study described above.

For assessment of rate effects, conventional microscopy, scanning electron microscopy (SEM), and transmission electron microscopy (TEM) were performed on corneal buttons, which were immediately harvested using 8-mm biopsy punches. For conventional microscopy, the buttons were dehydrated in a graded series of alcohol solutions. They were then cleared with xylene solution and fixed into a paraffin block. Corneal samples of 4- $\mu\text{m}$  thickness were sectioned and stained with hematoxylin and eosin (H&E). Light microscopy images were processed and stored for each sample. For TEM and SEM analysis, corneal buttons (four for each rate) were harvested and fixed in 2.5% glutaraldehyde in 0.1 M cacodylate buffer and prepared for analysis. The cornea buttons were bisected and postfixed in 2% osmium tetroxide for 2 hours. Small pieces of the cornea were embedded in low-viscosity epoxy medium, thin sectioned, stained with uranyl acetate and lead citrate, and viewed with a JEOL 100 CX transmission electron microscope. The other half of the cornea was prepared for SEM by critical point drying. The tissue was glued to stubs, sputter coated with gold palladium, and viewed with a JEOL 25 CF scanning electron microscope. SEM and TEM images were then processed and stored for each sample.

## RESULTS

### Ablation Plume Dynamics

The time evolution of the ablation plume is pictured in Figure 4. Each image is a single capture from the CCD camera. The reported time scale represents the delay of the image with respect to the surgical laser (Laser 1) pulse. Qualitatively, the bulk of the plume is observed to dissipate in less than 500 microseconds, and is essentially fully dissipated (98%) on a time-scale of about 3 milliseconds. To quantify the plume evolution, the intensity of each pixel was averaged across the entire image (1,024 $\times$ 1,024 pixels) and the background was subtracted for each time step, with the results plotted in Figure 5. This plot correlates well with the conclusions drawn from the images themselves and indicates a threshold of about 2–3 milliseconds, below which one would anticipate negligible interaction of the incident laser beam with the ablation plume from the previous pulse. At 400 Hz laser repetition rate, the pulse-to-pulse spacing is 2.5 milliseconds, which is consistent for this time scale, hence no significant effects are expected from interactions of the laser pulse with the bulk ablation plume for laser repetition rates up to 400 Hz.

To further corroborate the imaging studies in a more quantitative manner, transmission measurements were performed to ensure that the laser energy of the ablation beam is not attenuated by excess plume material lingering in the beam path. The transmission of the 193-nm probe laser is plotted in Figure 6 as a function of delay time following the ablating laser pulse (delay time of zero), hence the time axis represents the delay of the probe excimer beam (Laser 3) with respect to the ablation pulse (Laser 1). The transmission through the ablation plume was measured a minimum of three times for each delay using multiple eyes, with standard deviations included in Figure 6. The transmission profile shows a minimum of about 91% at a delay time between 120 and 250 microseconds, which corresponds to the passage of the bulk ablation debris through the probe beam at the probe beam height of 2 mm above the corneal surface, as shown in the plume imaging study (see Fig. 4). After the bulk of the plume evolves away, the transmission steadily climbs to 98.4%, rather than 100%. Examination of Figure 6 reveals that the transmission value of about 98.4% is persistent at the earliest delay times as well, namely between 1 and 10 microseconds. It is noted that these early times are well before the arrival of the bulk ablation plume. Additional measurements revealed that this decrease in transmission of the probe laser at early and late times is due to the build-up of a diffuse (presumably gaseous or very fine particulate) component of the ablation plume that persists over a time scale of tens of milliseconds. This diffuse component was observed at comparable levels (i.e.,  $\sim$ 98% transmission) for both 60 and 400 Hz. To further explore this effect, additional measurements were performed using a cross-flow purge at a fixed delay time of 1.25 milliseconds.

It was observed that adding a cross flow of dry nitrogen to purge the beam path allowed the transmission to reach unity at a time scale of 1.25 milliseconds. Transmission measurements were recorded for both laser repetition rates (60 and 400 Hz) with cross-flow added. The results are shown in Figure 7, for both 60 and 400 Hz. With the nitrogen purge flow, the transmission is increased to 1.00 ( $\sigma = 0.002$ ) and 1.00 ( $\sigma = 0.005$ ) for the 60- and 400-Hz experiments, respectively. Together, the data suggest that a diffuse, gas-phase component accumulates above the ablation surface and slightly attenuates the incoming laser pulse. However, no significant laser repetition rate effect is observed for this diffuse plume component. Clinically, this diffuse component is most likely diminished by the exhaust systems (i.e., plume extractors) that are present on commercial refractive systems, although the degree to which it might exist is difficult to predict. Given the small effect (1–2% attenuation) and the current findings, no rate dependence is expected over the range of 60–400 Hz examined here.

### Ablation Profile

Representative ablation profiles extracted from the white-light interferometry of the ablation craters are presented in Figure 8. For both laser repetition rates (60 and 400 Hz), five corneas were examined. As observed in

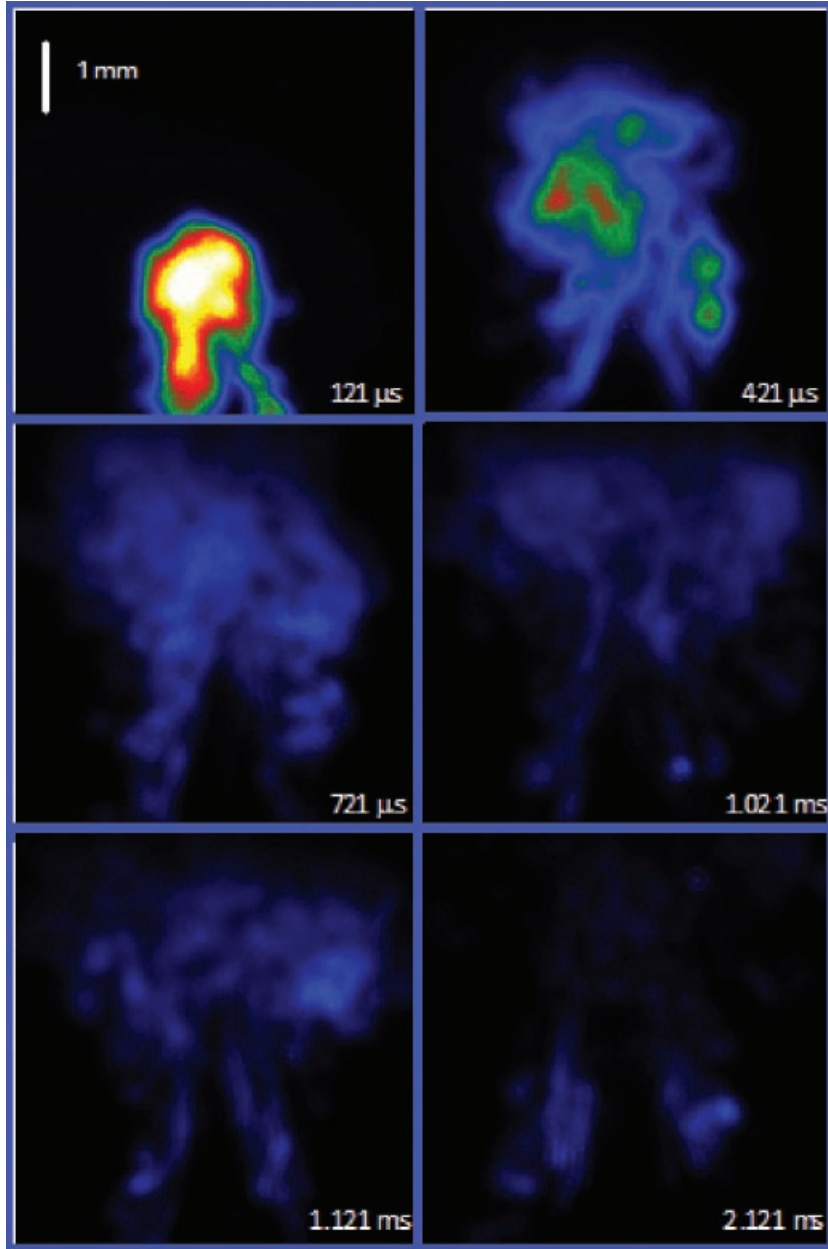


Fig. 4. Ablation plume images as a function of time following the ablating laser pulse. All images have the same intensity scale.

the figure, there is no obvious change in the ablation crater geometry across the entire profile with laser repetition rate. Specifically, the edges of the ablation zone profile line up with each other for the two treatment rates, as do the bottoms of the crater in the corneal bed, showing similarity in ablation rates at both the maximum fluence (i.e., center) and the near-threshold fluence (i.e., edge). The ablation profile as defined here corresponds to the 25-shot crater superimposed on the overall treatment; hence the scanning approach depicted in Figure 3. The average ablation full-depth is defined by the maximum depth of the ablation

profile, and the ablation rate is defined as the ablation full-depth divided by the number of pulses used to create the profile.

The average ablation full-depth at 60 Hz is  $23.6 \mu\text{m}$  ( $\sigma = 1.98 \mu\text{m}$ ), and the average ablation full-depth at 400 Hz is  $23.1 \mu\text{m}$  ( $\sigma = 2.93 \mu\text{m}$ ), as shown in Figure 9, which corresponds to ablation rates of  $0.944$  and  $0.924 \mu\text{m/pulse}$  at crater center, respectively. For a 95% confidence value using the Student's *t*-test, there is no statistical difference in ablation depths for the 60 and 400 Hz rates. In summary, both the depth and overall shape of the ablation craters are

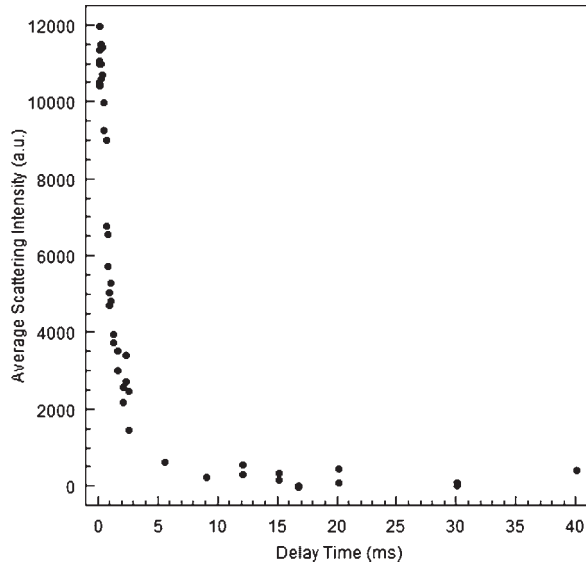


Fig. 5. Average scattering intensity (full-image) of the ablation plume images as a function of time following the ablating laser pulse.

unaltered with changes in the laser repetition rate, leading to the conclusion of no measurable repetition rate effect on the resulting profiles.

The peak fluence of the surgical laser in these experiments is approximately  $600 \text{ mJ/cm}^2$ , while the average

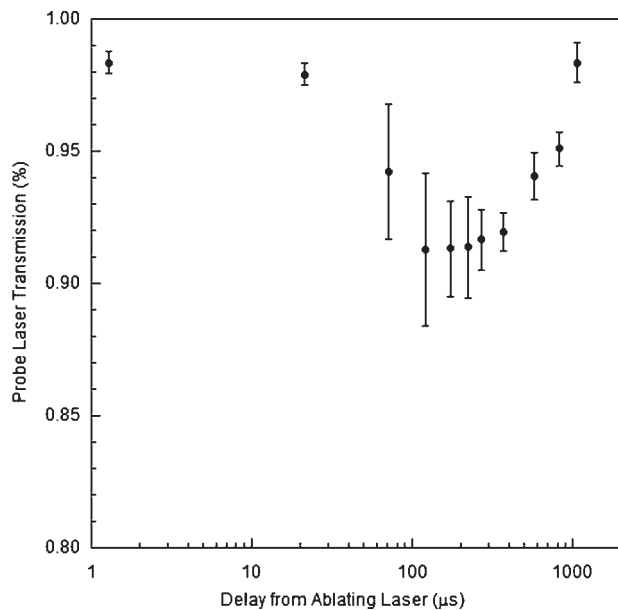


Fig. 6. One hundred ninety-three nanometer ArF probe laser transmission through the ablation plume as a function of time following ablation. Transmission was recorded at a fixed height of 2 mm above cornea surface.

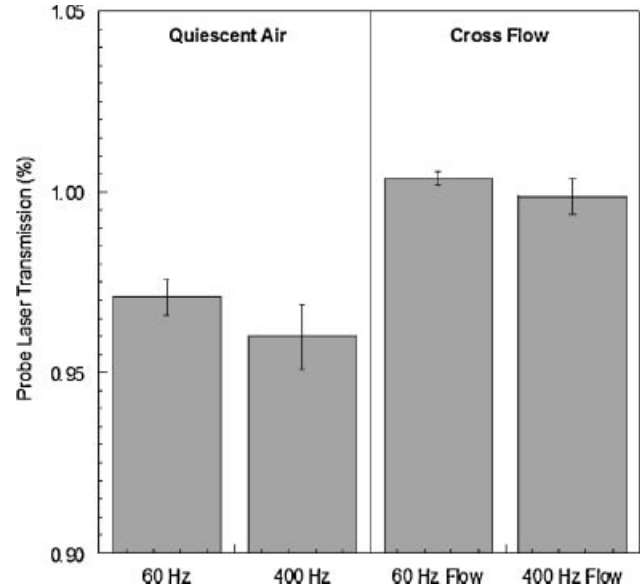


Fig. 7. Average transmission of the ArF probe laser at a fixed delay of 1.25 ms and fixed height of 2 mm. Data were recorded in quiescent air, and in the presence of a nitrogen cross flow oriented orthogonal to the probe laser beam.

fluence (full-width) is approximately  $200 \text{ mJ/cm}^2$ . The corresponding ablation rates for 60- and 400-Hz ablations, namely  $0.94$  and  $0.92 \text{ }\mu\text{m/pulse}$ , agree very well with previously published values in the range of approximately  $0.8\text{--}1.3 \text{ }\mu\text{m/pulse}$  over this fluence range [10,17–25].

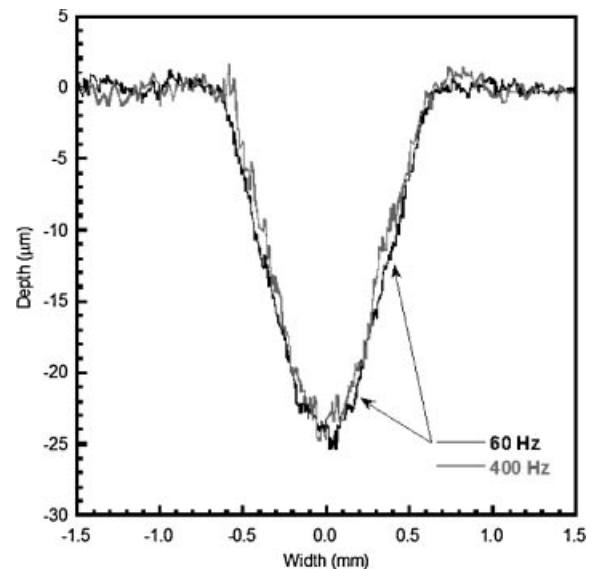


Fig. 8. Representative ablation crater profiles recorded using a 25-shot sequence superimposed over a standard 3-diopter correction at 60 and 400 Hz. Profiles were recorded from wax impressions made immediately following the ablation. Note that the width is in millimeters, while the depth is in micrometers.

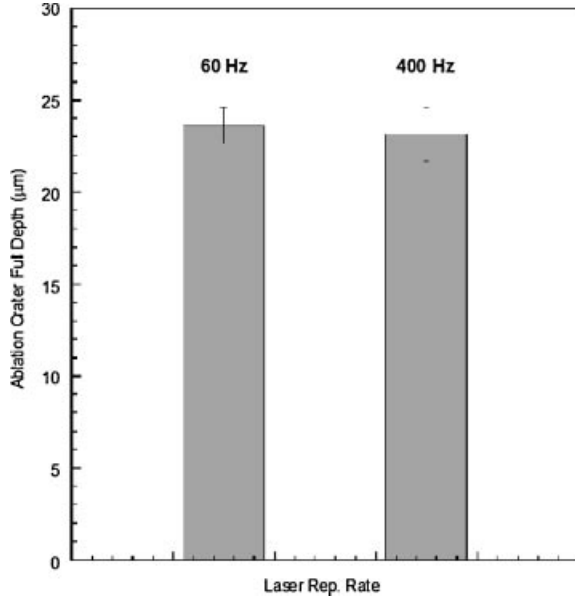


Fig. 9. Average ablation crater full-depths ( $N=5$ ) recorded using a 25-shot sequence superimposed over a standard 3-diopter correction. Ablations were performed at 60 and 400 Hz repetition rates.

### Histology

Conventional light microscopy images from the extracted corneal buttons are shown in Figure 10. Qualitatively, no differences are observed between the samples generated at 60 Hz and those generated at 400 Hz.

To provide higher magnification, SEM images of the extracted corneas ablated at 60 and 400 Hz were generated and are shown in Figure 11 at various magnifications. When comparing comparable conditions for the image pairs, both ablation conditions (60- and 400-Hz laser repetition rate) appear to present similar features, suggesting that no differential response exists between the two ablation conditions within the ablation bed. The only notable difference is a slightly greater roughness in the 60 Hz ablations images. This difference was not further

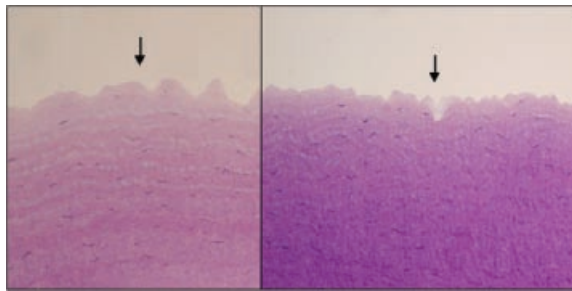


Fig. 10. High magnification microscopy images of the ablation crater for laser ablations created at 60 Hz (left) and 400 Hz (right). The upper surface (as indicated by the arrows) indicates the treatment (i.e., ablation) surface.

investigated in a quantitative manner, nor was a similar trend noted in the TEM analysis.

In order to quantitatively assess any ablation rate effects, TEM analysis was performed to directly image the collagen fibrils. As with the SEM microscopy, TEM was performed at the sides and bottoms of the ablation craters. TEM images of corneas ablated at 60 and 400 Hz are shown in Figure 12 at the same magnification for direct comparison. Just as with the SEM images, no additional tissue damage is visually noticeable, including no visually observable condensing or distortion of collagen fibrils. As shown by the scale bars in Figure 12, the collagen fibers are characterized by an average diameter of about 30 nm, as consistent with the literature values. The TEM analysis revealed no differential damage between the two ablation rates based on the observed structures. As observed in the inset of Figure 12, the individual fibrils appear cleanly severed at the ablation surface. One interesting feature of the TEM images is the appearance of a diffuse, “dust like” layer on the ablation zone surface. This layer has a thickness on the order of 100 nm, and was persistent on all ablated surfaces. The exact nature of this layer remains undetermined, but most likely consists of collagen debris.

In order to quantify information that may be represented in the TEM images, the configuration of collagen fibrils at the ablation surface was examined more closely. The TEM images (three eyes for each rate) were broken into squares normal to the ablated crater surface, and the number of collagen fibrils (i.e., dots) in each square was counted. The counts (corrected for varying magnifications) were then compared. At 60 Hz, an average of 221 fibrils/ $\mu\text{m}^2$  ( $\sigma = 36$  fibrils/ $\mu\text{m}^2$ ) were observed adjacent to the ablation surface. At 400 Hz, an average of 263 fibrils/ $\mu\text{m}^2$  ( $\sigma = 22$  fibrils/ $\mu\text{m}^2$ ) were observed. For a 95% confidence value (Student’s *t*-test), there is no statistical difference in collagen fibril density near the ablation surface between 60 and 400 Hz ablation rates. Additionally, no measurable difference in fiber diameter (size) was found. Overall, the collagen fibrils do not show any signs of disorganization, size changes or coagulation. Based on the SEM and TEM analysis, it is concluded that no thermal damage or differential thermal damage (i.e., 60 Hz vs. 400 Hz) is observed under these ablation conditions.

### DISCUSSION

The current experiments have examined the potential effects of laser repetition rate on corneal ablation over a range of clinically relevant conditions. Experiments have assessed a comprehensive range of parameters, including plume dynamics, corneal ablation profiles, and high-resolution microscopy of collagen structure, which in aggregate lead to the conclusion that no observable effects of laser repetition rate are present for the comparison of 60 and 400 Hz.

Direct comparisons with previous plume dynamics studies are difficult, as each study uses a specific set of experimental conditions, namely fluence, wavelength and laser beam diameter (spot size). However, the trends noted

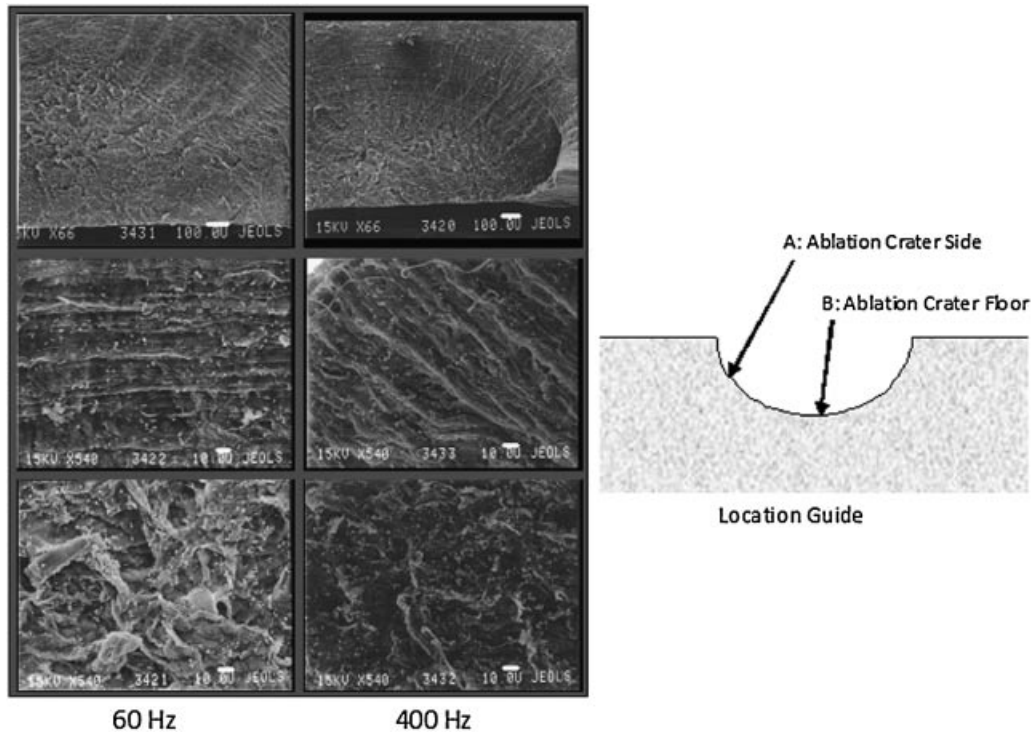


Fig. 11. SEM images of the overall ablation crater (top row), the ablation crater sides (middle row = A), and the floor of the ablation crater (bottom row = B), for ablations recorded at 60 Hz (left) and 400 Hz (right). Scale bars are included in each frame, with the actual scale length listed below in microns.

here are consistent with the literature. The early images of Puliafito et al. [33] show a similar plume evolution scheme with quicker dissipation than was noted here, which is expected due to the higher laser fluence used. The time-scales are also very consistent with the plume velocities on the order of 10 m/seconds reported by Hahn et al. [36] for an

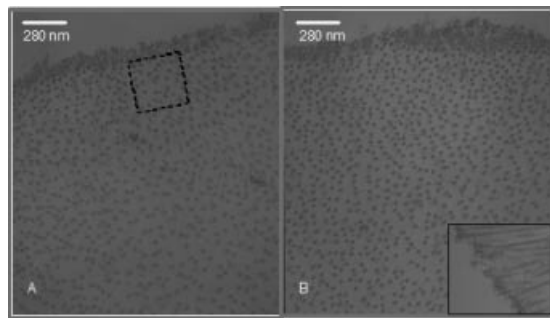


Fig. 12. TEM images of bovine cornea cross-sections following laser ablation at 60 Hz (left) and 400 Hz (right). The upper surface is the ablation surface, and the individual collagen fibrils are visible in cross-section. The scale bar is 280 nm. **Panel A** shows a representative grid used for collagen fiber counting. The insert in **Panel B** shows a transverse section of collagen fibrils at the surface.

average (full-beam) fluence of 100 mJ/pulse. Noack et al. [16] reported that laser shielding by build-up of plume material is significant for large beams, noting that plumes generated by smaller diameter laser beams (e.g.,  $\sim 1$  mm) dissipate much quicker than their large diameter counterparts. The current study has found that laser shielding is insignificant for ablation with a 1-mm spot size at rates up to approximately 400 Hz. Pettit and Ediger found that the transmission through the ablation plume and excised cornea combined was minimized at 30 microseconds at a value of 40% [37]. It is not expected that the reported transmission values match those determined here, as their probe wavelength was 355 nm and the pathlength included the actual cornea itself, which is highly absorbing in the UV region. However, the evolution of transmission over time is consistent with the current findings. From their data, it appears that they also observed the lack of resolution of transmission to 100% at longer time scales.

In addition to plume considerations, the measured ablation profiles, overall ablation depths and ablation rates were statistically identical for ablations generated with laser repetition rates 60 Hz and 400 Hz. Additionally, the ablation rates determined in this study (0.94 and 0.92  $\mu\text{m}/\text{pulse}$ ) are consistent with those previously reported values (0.8–1.3  $\mu\text{m}/\text{pulse}$ ) for the 600  $\text{mJ}/\text{cm}^2$  fluence range [10,17–25] further corroborating the current values.

The exact mechanism of photoablation remains a topic of research [6,38]. Several interesting findings in the current study are relevant and provide insight as to the overall process of excimer laser ablation of corneal tissue, namely the TEM analysis and the transmission experiments. First the finding of a persistent, diffuse component of the ablation plume (see Fig. 6), as measured by 193-nm absorption, suggests molecular fragments from the ablation process itself. This finding is supportive of a photochemical mechanism, in which amino acid fragments are created within the tissue matrix and subsequently ejected with the plume. Second, the lack of any noticeable damage or perturbation to the collagen fibrils immediately underlying the ablation zone, as seen in the TEM histology experiments, speaks to the precision of excimer laser tissue etching. The lack of any indication of thermal damage in the microscopy images is consistent with a photochemical process. Together, such results are in agreement with a photochemical model of ArF laser ablation of corneal stromal tissue, in which the high excimer laser photon energy (6.4 eV) can directly cleave protein strands (i.e., peptide bonds), forming transient species, in a very dynamic laser-tissue interaction process [10].

Ishihara et al. have studied the surface temperature of cornea during ablation, and found that the peak surface temperature increases with laser fluence [39,40]. At 180 mJ/cm<sup>2</sup>, they reported a value of 240°C surface temperature, and at fluences near 300 mJ/cm<sup>2</sup>, the temperature is as high as approximately 325°C. These results suggest a photothermal component to the ablation mechanism. However, additional measurements by this group determined that the increase in temperature decreases rapidly on a time scale of a few hundred microseconds for 193-nm irradiation. This quick dissipation of surface temperature supports the current findings of no differential thermal damage, as the pulse-pulse time scale is on the order of several ms. Thusly, the thermal energy is expected to dissipate on a time scale much less than that of the laser repetition rate. Ishihara and coworkers also found that the surface temperature relaxes more quickly for 193-nm irradiation as compared to 248-nm irradiation [40], concluding that the thermal component of ablation is considered to increase with increasing wavelength, notably so in the infrared spectral region. Overall, the reduced surface temperature observed with 193-nm irradiation seems to indicate a mechanism that is less reliant on thermal excitation.

Additional insight into the present findings may be gained by contrasting the results with a previous study of laser repetition rate effects of CO<sub>2</sub> lasers on tissue. The ablation mechanism of CO<sub>2</sub> laser-tissue interaction is considered a purely thermal process. For this type of ablation, thermal damage and the resulting ablation rate have been found to significantly increase with laser repetition rate [41,42]. This is in stark contrast to the results of the current study, which do not indicate any differential tissue damage or a change in ablation depth with repetition rate. This difference may be explained in part in the context of thermal relaxation times. The relaxation time is on the order of tens of ms for the case of

CO<sub>2</sub> ablation [32], and may be estimated to be on the order of tens of microseconds for 193-nm ablation based on the increased absorption coefficient. Thus, based on the thermal relaxation criterion, one may estimate a critical laser repetition rate for 193-nm excimer laser ablation that is in the range of kilohertz, much greater than the range examined in the current study. This is consistent with the current findings of no differential thermal tissue damage, although the exact partitioning between photochemical and photothermal processes remains uncertain for the deep UV wavelength region (e.g., 193 nm). The TEM analysis and the well-defined nature of the ablation craters (including thresholds) are also consistent with a significant photochemical ablation component with the 193-nm excimer, which is in agreement with the recent comprehensive review by Vogel and Venugopalan [6].

In summary, investigation of the relative effects of excimer laser repetition rate on the overall corneal ablation processes (i.e., plume dynamics, ablation rates and corneal pathology) revealed no measurable difference under conditions typical of refractive procedures. This study suggests that increases in ArF laser repetition rates for clinical applications (up to ~400 Hz) appear feasible, and therefore justify the pursuit of additional clinical studies.

## ACKNOWLEDGMENTS

This work was supported in part (LMS and DWH) by a grant from Alcon Research, Ltd. and in part (HFE) by NEI grants R01-EY00933 and P30-EY06360. Any opinions, findings, and conclusions expressed in this article are those of the authors and do not necessarily reflect views of the sponsors.

## REFERENCES

1. <http://www.fda.gov/cdrh/LASIK/lasers htm>, updated March 6, 2008.
2. Stein HA, Cheskes AT, Stein RM. Current internationally available models. In: *The excimer: Fundamentals and clinical use*. New Jersey: SLACK inc; 1997. 13–25.
3. Fisher BT, Hahn DW. Measurement of small-signal absorption cross section of collagen for 193-nm excimer laser light and the role of collagen in tissue ablation. *Appl Opt* 2004; 43:5443–5451.
4. Jimenez JR, Rodriguez-Marin F, Anera RG, Jimenez del Barco L. Deviations of Lambert-Beer's law affect corneal refractive parameters after refractive surgery. *Opt Express* 2006;14:5411–5417.
5. Nikosgosyan DN, Gerner H. Laser induced photodecomposition of amino acids and peptides: Extrapolation to corneal collagen. *IEEE J Quantum Elect* 1999;5:1107–1115.
6. Vogel A, Venugopalan V. Mechanisms of pulsed laser ablation of biological tissues. *Chem Rev* 2003;103:577–644.
7. Paltauf G, Dyer PE. Photomechanical processes and effects in ablation. *Chem Rev* 2003;103:577–644.
8. Manns F, Milne P, Parel JM. Ultraviolet corneal photoablation. *J Refract Surg* 2002;8:1–5.
9. Hu XH, Fang Q, Cariveau MJ, Pan X, Kalmus GW. Mechanism study of porcine skin ablation by nanosecond laser pulses at 1064, 532 266, and 213 nm. *IEEE J Quantum Elect* 2001;37:322–328.
10. Fisher BT, Hahn DW. Development and numerical solution of a mechanistic model for corneal tissue ablation with the 193 nm argon fluoride excimer laser. *J Opt Soc Am A* 2007; 24:265–277.

11. Pettit GH, Sauerbrey R. Pulsed ultraviolet laser ablation. *Appl Phys A* 1993;56:51–63.
12. Tokarev VN, Lunney JG, Marine W, Sentis M. Analytical thermal model of ultraviolet laser ablation with single-photon absorption in the plume. *J Appl Phys* 1995;78:1241–1246.
13. Sutcliffe E, Srinivasan R. Dynamics of UV laser ablation of organic polymer surfaces. *J Appl Phys* 1986;60:3315–3322.
14. Srinivasan R, Braren B, Seeger DE, Dreyfus RW. Photochemical cleavage of a polymeric solid—Details of the ultraviolet-laser ablation of poly(methyl methacrylate) at 193-nm and 248-nm. *Macromolecules* 1986;19:916–921.
15. Munnerlyn CR, Arnoldussen ME, Munnerly AL, Logan BA. Theory concerning the ablation of corneal tissue with large-area, 193-nm excimer laser beams. *J Biomed Opt* 2006;11:32–64.
16. Noack J, Tonnies R, Hohla K, Birngruber R, Vogel A. Influence of ablation plume dynamics on the formation of central islands in excimer laser photorefractive keratectomy. *Ophthalmology* 1997;104:823–830.
17. Puliafito CA, Wong K, Steinert RF. Quantitative and ultrastructural studies of excimer laser ablation of the cornea at 193 and 248 nanometers. *Lasers Surg Med* 1987;7:155–159.
18. Aron-Rosa DS, Boulnoy JL, Carre F, Delacour J, Gross M, Lacour M, Olivo JC, Timsit JC. Excimer laser surgery of the cornea: Qualitative and quantitative aspects of photoablation according to the energy density. *J Cataract Refr Surg* 1986;12:27–33.
19. Berns MW, Chao L, Giebel AW, Liaw LH, Andrews J, VerSteege B. Human corneal ablation threshold using the 193-nm ArF excimer laser. *Invest Ophthalmol Vis Sci* 1999;40:826–830.
20. Campos M, Wang XW, Hertzog L, Lee M, Clapham T, Trokel SL, McDonnell PJ. Ablation rates and surface ultrastructure of 193 nm excimer laser keratectomies. *Invest Ophthalmol Vis Sci* 1993;34:2493–2500.
21. Fantes FE, Waring GO. Effect of excimer laser radiant exposure on uniformity of ablated corneal surface. *Lasers Surg Med* 1989;9:533–542.
22. Huebscher HJ, Genth U, Seiler T. Determination of excimer laser ablation rate of the human cornea using in vivo Scheimpflug videography. *Invest Ophthalmol Vis Sci* 1996;37:42–46.
23. Kitai MS, Popkov VL, Semshishen VA, Kharizov AA. The physics of UV laser cornea ablation. *IEEE J Quantum Elect* 1991;27:302–307.
24. Krueger RR, Trokel SL. Quantitation of corneal ablation by ultraviolet laser light. *Arch Ophthalmol* 1985;103:1741–1742.
25. Van Saarloos PP, Constable IJ. Bovine corneal stroma ablation rate with 193-nm excimer laser radiation: Quantitative measurement. *Refract Corneal Surg* 1990;6:424–429.
26. Lerman S. The cornea. In: *Radiant energy and the eye*. New York: Macmillan Publishing Co., Inc; 1980. 43–59.
27. Niemz MH. Medical applications in lasers. In: *Laser-tissue interactions*. New York: Springer; 1996. 162–177.
28. Klyce SD, Beuerman RW. Structure and function of the cornea. In: Krachmer J, Palay D, editors. *The cornea*. New York: Churchill Livingstone; 1998. 3–54.
29. Boote C, Dennis S, Newton RH, Puri H, Meek KM. Collagen fibrils appear more closely packed in the prepupillary cornea: Optical and biomechanical implications. *Invest Ophthalmol Vis Sci* 2003;44:2941–2948.
30. Niemz MH. Interaction mechanisms. In: *Laser-tissue interactions*. New York: Springer; 1996. 77–80.
31. Pearce J, Thomsen S. Rate process analysis of thermal damage. In: Welch AJ, van Gemert MJC, editors. *Optical-thermal response of laser-irradiated tissue*. New York: Plenum Press; 1995. 570–584.
32. Venugopalan V, Nishioka NS, Mikic BB. The effect of laser parameters on the zone of thermal injury produced by laser ablation of biological tissue. *J Biomech Eng Trans ASME* 1994;116:62–70.
33. Puliafito CA, Stern D, Krueger RR, Mandel ER. High-Speed photography of excimer laser ablation of the cornea. *Arch Ophthalmol* 1987;105:1255–1259.
34. Nahen K, Vogel A. Plume dynamics and shielding by the ablation plume during Er:YAG laser ablation. *J Biomed Opt* 2002;7:165–178.
35. Fisher BT, Hahn DW. Determination of excimer laser ablation rates of corneal tissue using wax impressions of ablation crater and white-light interferometry. *Ophthalmic Surg Lasers Imaging* 2004;35:41–51.
36. Hahn DW, Ediger MN, Pettit GH. Dynamics of ablation plume particles generated during excimer laser corneal ablation. *Laser Surg Med* 1995;16:184–389.
37. Pettit GH, Ediger MN. Pump/probe transmission measurements of corneal tissue during excimer laser ablation. *Laser Surg Med* 1993;13:363–367.
38. Venugopalan V, Nishioka NS, Mikic BB. The thermodynamic response of soft biological tissue to pulsed ultraviolet laser irradiation. *Biophys J* 1995;69:1259–1271.
39. Ishihara M, Arai T, Sato S, Morimoto Y, Obara M, Kikuchi M. Measurement of the surface temperature of the cornea during ArF excimer laser ablation by thermal radiometry with a 15-nanosecond time response. *Laser Surg Med* 2002;30:54–59.
40. Ishihara M, Arai T, Sato S, Morimoto Y, Obara M, Kikuchi M. Nanosecond-time-response temperature measurements using radiation thermometry during 193 nm and 247 nm pulsed light irradiation: Comparison of corneal surface temperature histories. *Proc SPIE* 2001;4257:298–302.
41. Venugopalan V, Nishioka NS, Mikic BB. The effect of CO<sub>2</sub> laser pulse repetition rate on tissue ablation rate and thermal damage. *IEEE T Bio-Med Eng* 1991;38:1049–1052.
42. Gerstmann M, Sagi A, Avidor-Zehavi A, Katzir A, Akselrod S. Model simulation of biological damage in tissue exposed to CO<sub>2</sub> laser irradiation. *Opt Eng* 1993;32:291–297.
43. Noack J, Tonnies R, Hohla K, Birngruber R. Influence of ablation plume dynamics on the formation of central islands in excimer laser photorefractive keratectomy. *Ophthalmology* 1997;104:823–830.
44. Ishihara M, Arai T, Sato S, Nakano H, Obara M, Kikuchi M. Temperature monitoring by infrared radiation measurements during ArF excimer laser ablation with cornea. *Proc SPIE* 1999;3601:335–339.